






# Focal Surface Detection of High Numerical Aperture Objective Lens Based on Differential Astigmatic Method

Jia-Lin Du , Wei Yan , Li-Wei Liu, Fan-Xing Li , Fu-Ping Peng , Si-Mo Wang , Si-Yang Yu, and Jian Wang

**Abstract**—Defocus detection technology is the key technology in the fields of laser direct writing, optical disc storage, and high-precision lithography, which directly affects the accuracy of line drawing. In this paper, using the principle of astigmatic method, combined with differential technology, a nano-level defocus detection method based on differential astigmatism for the high numerical aperture systems is proposed. Firstly, by establishing a mathematical model, the theoretical analysis and simulation of the defocus detection method based on differential astigmatism are carried out. In addition, the system parameters at the maximum sensitivity of the high numerical aperture defocus detection system is also solved. Secondly, the defocus detection experimental system based on astigmatic method was built for experimental demonstration. Finally, using the objective lens with a numerical aperture of 0.8, the focus error signal curve with a good linear relationship is obtained in this paper. The linear range is  $6\mu\text{m}$ ; the system sensitivity can reach 5 nm; the system detection accuracy is 30 nm, and the repeat positioning accuracy can reach 30 nm. The defocus detection method based on the high numerical aperture objective lens has the advantages of large detection range, high detection accuracy and compact system structure, which can be widely used in various new high-precision laser processing fields.

**Index Terms**—Astigmatic method, differential technology, high numerical aperture, high sensitivity.

## I. INTRODUCTION

**I**N ORDER to portray high-precision lines, high numerical aperture (NA) objective lenses are widely used in laser direct writing, optical disc storage and high-precision lithography [1]–[6]. The use of high numerical aperture and short focal depth objectives puts forward new requirements for defocus error detection technology [7]. The basic principle of defocus error detection is to establish the relationship between the defocus

amount of the sample and the intensity or shape change of the light spot on the detector through the defocus detection element. And through the corresponding processing method, the linear relationship between the focus error signal and the defocus amount is obtained. The current defocus error detection methods mainly include astigmatic method, critical angle method, Foucault knife-edge method, decentered beam method, pinhole focusing method, etc. [8], [9]. The astigmatic method is widely used in high-precision defocus detection due to its simple structure and high resolution [10], [11]. Its basic principle is to use the astigmatic elements to change the energy distribution of the laser beam returning from the sample, thereby forming spots of different shapes on the detector, and establishing the relationship between the defocusing amount of the sample and the energy distribution of the detector spot [11]–[14]. By measuring the focus error signal on the detector, the defocus amount of the sample can be calculated.

At present, the research on the astigmatism defocus detection technology has made good progress. Li Y et al. established a high-precision displacement measurement system based on the astigmatic method, achieving a detection accuracy of 0.1  $\mu\text{m}$  [9], [15], [16]; Tian Yiqiang and Chen Li et al. analyzed the influence of the parameters of the astigmatism and defocus detection system on the amount of defocus, sensitivity and spot size, and proposed the optimization and design principles of the system parameters [17], [18]. The above-mentioned research mainly focuses on focusing systems with low numerical aperture. However, with the wide application of high numerical aperture systems, the current research on focal plane detection accuracy of 100nm-level is difficult to cope with the defocus detection of high numerical aperture systems [19], [20]. For example: for the focus of the vector light field, use an objective lens with a numerical aperture (NA) of 1.4, and from the formula  $DOF = 0.5\lambda/(NA)^2$ , it can be seen that for a system with a laser beam wavelength  $\lambda$  of 365nm, the focal depth  $DOF$  is lower than 100nm [11], [14], [21]–[23]. Therefore, for a high NA system, it is necessary to design its system parameters reasonably to improve the accuracy of its defocus detection to the nanometer level.

In the field of high-precision focal plane detection, the stability, noise resistance and adaptability of the detection system to the measured surface also have a great influence on the performance of the detection system. Since the astigmatic method uses a single four-quadrant detector to collect the light

Manuscript received May 17, 2021; revised June 24, 2021; accepted July 11, 2021. Date of publication July 14, 2021; date of current version August 18, 2021. This work was supported in part by the Instrument Development of Chinese Academy of Sciences under Grants YJKYYQ20180008, and YJKYYQ20180006, and in part by the Sichuan Science and Technology Program under Grants 2020JDJQ0007, 2021JDRC0089, and 2021JDRC0084. (Corresponding author: Wei Yan.)

Wei Yan, Fan-Xing Li, Si-Yang Yu, and Jian Wang are with the Institute of Optics and Electronics, Chinese Academy of Sciences, Chengdu 610209, China (e-mail: yanwei@ioe.ac.cn; lifanxing15@mails.ucas.ac.cn; yusiyang@ioe.ac.cn; wjlx@my.swjtu.edu.cn).

Jia-Lin Du, Li-Wei Liu, Fu-Ping Peng, and Si-Mo Wang are with the Institute of Optics and Electronics, Chinese Academy of Sciences, Chengdu 610209, China and also with the University of Chinese Academy of Sciences, Beijing 100049, China (e-mail: dujialin18@mails.ucas.ac.cn; liuliwei18@mails.ucas.ac.cn; pengfuping16@mails.ucas.ac.cn; wangsimo18@mails.ucas.ac.cn).

Digital Object Identifier 10.1109/JPHOT.2021.3097086

intensity to obtain the defocus signal, the stray light and the airflow disturbance of the external environment have a bad influence on its stability and noise [24], [25]. The differential technology has the advantages of improving the system sensitivity and suppressing system noise [25]–[28]. Therefore, based on the principle of differential technology, the defocus signal is collected by two detectors, and the difference between the two detection signals is used to express the defocus information, so as to suppress the influence of environmental fluctuations and stray light on the detection signal, and improve the stability and noise immunity of the detection system.

In addition to the important indicators such as defocus detection accuracy and stability, repeat positioning accuracy and sensitivity are also important parameters to ensure the quality of the depicted lines. At present, most of the literature only studies the influencing factors of the defocus detection range, detection accuracy and the optimization design of the focal plane detection system parameters, while ignoring the discussion of the repeated positioning accuracy and maximum sensitivity of the detection system [11], [14], [15], [17], [18]. Therefore, for high-precision lithography, while meeting the feasibility requirements of the defocus detection range and spot size, and the compactness of the system structure, it is necessary to optimize the design of the defocus detection system parameters to solve the maximum sensitivity. And through the measurement of static repeatability positioning and dynamic repeatability positioning, the defocus detection system is evaluated.

Therefore, based on the theory of astigmatism, combined with differential technology, this paper proposes a defocus detection method based on the differential astigmatic method, and conducts theoretical research and simulation analysis on the high NA system. The simulation analysis solves the system parameters at the maximum sensitivity of the system on the basis of taking into account the practical feasibility. Finally, an experimental platform was built to demonstrate, and the sensitivity, repeat positioning accuracy and stability of the system were tested. The results show that for the objective lens with a numerical aperture of 0.8, the linear range of the experimental system can reach more than  $6\mu\text{m}$ ; the sensitivity of the system is 5 nm; the detection accuracy of the system reaches 30 nm; and the repeat positioning accuracy can reach 30 nm. The research results of this paper show that, under the premise of considering feasibility and experimental requirements, the defocus detection system based on the differential astigmatic method can be applied to the field of new high-precision lithography machines.

## II. PRINCIPLE AND MODEL

### A. Principle of Astigmatic Method

The schematic diagram of the astigmatism method is shown in Fig. 1(a). The combination of spherical lens ( $L_0$ ) and cylindrical lens ( $CL_0$ ) is used as the astigmatic element. Since the cylindrical lens only has a focusing effect on the meridian plane, there is a difference in the focusing ability of the meridian plane and the sagittal plane during imaging, so that the meridian focal line ( $t$ ) and the sagittal focal line ( $s$ ) are formed behind the cylindrical lens. The shape of the spot between the two focal lines gradually

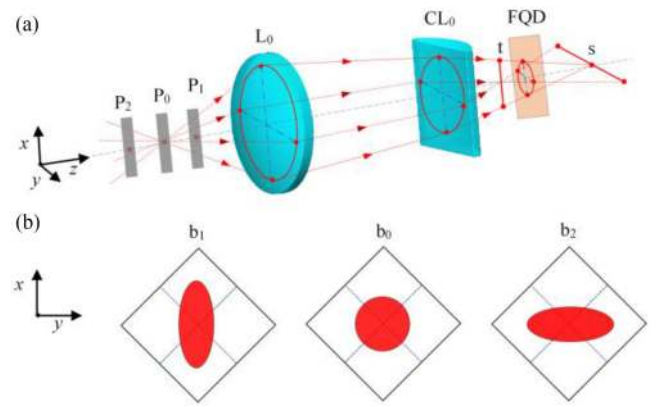


Fig. 1. Schematic diagram of the principle of astigmatism. (a) Optical path. (b) Light field distribution on FQD.

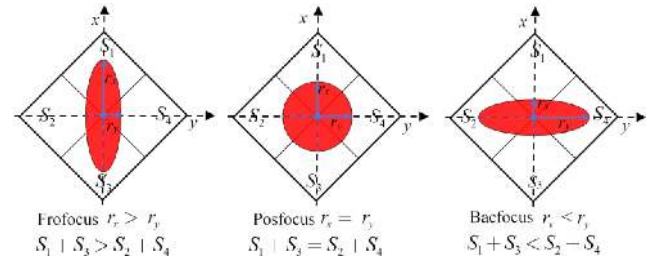


Fig. 2. Detection principle diagram of the FQD.

changes from a vertical ellipse to a horizontal ellipse, that is, the energy distribution of the spot on the  $x$ -axis and  $y$ -axis changes continuously along the optical axis. Therefore, the four-quadrant detector (FQD) is used as the signal detection element to detect the energy distribution of the spot at a specific position between the two focal lines, and the defocus direction and defocus size of the sample can be determined.

Due to the specific relationship between the image surface light field energy distribution and the axial position of the sample, the position where the image side light field distribution is circular is defined as the positive focus position  $P_0$  (called “Posfocus”), as shown in Fig. 1(b- $b_0$ ). When the sample is out of focus and at the position  $P_1$  (called “Frofocus”, it is in front of the focal plane), the image side light field distribution is a vertical ellipse as shown in Fig. 1(b- $b_1$ ); when the sample is at the position  $P_2$  (called “Bacfocus”, it is in front of the focal plane), the image side light field distribution is a horizontal ellipse as shown in Fig. 1(b- $b_2$ ).

The detection principle of the FQD is shown in Fig. 2. The spot energy is divided into four parts:  $S_1$ ,  $S_2$ ,  $S_3$ , and  $S_4$ , the intensities of which are respectively  $I_1$ ,  $I_2$ ,  $I_3$ , and  $I_4$ , and the total energy is  $I_0$ . When the sample is in the positive focus position, the light field distribution on the detector is circular. At this time, the energy of the light spots in the four quadrants of  $S_1$ ,  $S_2$ ,  $S_3$ , and  $S_4$  are completely equal. When the sample is at the Frofocus position or the Bacfocus position, the light field distribution on the detector changes to an ellipse, and the spot energy in the four quadrants  $S_1$ ,  $S_2$ ,  $S_3$ , and  $S_4$  is not equal. Therefore, the focus

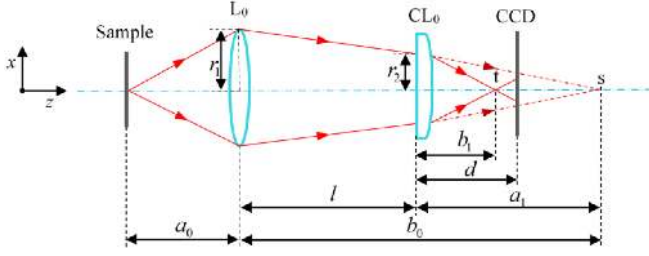


Fig. 3. Schematic diagram of astigmatic method optical path.

error signal ( $FES$ ) can be defined as follows:

$$FES = \frac{(I_1 + I_3) - (I_2 + I_4)}{I_1 + I_2 + I_3 + I_4} = \frac{(I_1 + I_3) - (I_2 + I_4)}{I_0} \quad (1)$$

Assuming that the energy distribution of the light field on the detector is uniform and symmetric; then, one can get:

$$I_i = CS_i, \quad (i = 1, 2, 3, 4) \quad (2)$$

$$S_1 = S_3, \quad S_2 = S_4 \quad (3)$$

Where  $C$  is constant. Based on the formula of the geometric area of the elliptical spot,  $S_1$ ,  $S_2$ ,  $S_3$ , and  $S_4$  can be calculated as follows:

$$S_1 = S_3 = \frac{\pi r_x r_y}{2} - r_x r_y \arcsin \left( \frac{|r_y|}{\sqrt{r_x^2 + r_y^2}} \right),$$

$$S_2 = S_4 = r_x r_y \arcsin \left( \frac{|r_y|}{\sqrt{r_x^2 + r_y^2}} \right) \quad (4)$$

Where  $r_x$  and  $r_y$  are the  $x$ -axis and  $y$ -axis radius of the detector FQD, respectively. Combining formulas (1)–(4), the focus error signal ( $FES$ ) can be calculated as:

$$FES = 1 - \frac{4}{\pi} \arcsin \left( \frac{|r_y|}{\sqrt{r_x^2 + r_y^2}} \right) \quad (5)$$

Equation (5) shows that there are three special points about the  $FES$ : when  $r_x = r_y$ ,  $FES = 0$ , the optical field distribution on the detector is circular; when  $r_y = 0$ ,  $FES = 1$ , the optical field distribution on the detector is a vertical focal line; when  $r_x = 0$ ,  $FES = -1$ , and the light field distribution on the detector is a horizontal focal line. The values of  $r_x$  and  $r_y$  can be obtained by the principle of geometric optical imaging, which will be derived next.

The schematic diagram of the astigmatic method optical path is shown in Fig. 3.  $a_0$  and  $b_0$  are the object and image distances of the objective lens ( $L_0$ ), respectively.  $a_1$  and  $b_1$  are the object and image distances of the cylindrical lens ( $CL_0$ ), respectively. The distance between the two lenses is  $l$ , and the distance between the  $CL_0$  and the detector CCD is  $d$ . The focal lengths of the  $L_0$  and the  $CL_0$  are  $f_1$  and  $f_2$ , respectively. Combined with Gaussian formula, one can get:

$$\frac{1}{b_0} + \frac{1}{a_0} = \frac{1}{f_1}, \quad \frac{1}{b_1} - \frac{1}{a_1} = \frac{1}{f_2} \quad (6)$$

Assuming that the radius of the  $L_0$  and the  $CL_0$  are  $r_1$  and  $r_2$ , respectively. the geometric similarity relationship can be used

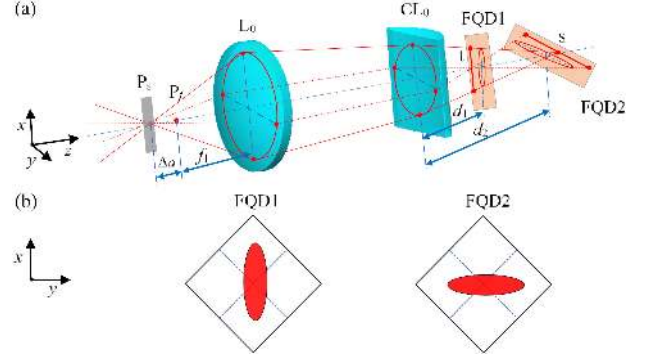


Fig. 4. Schematic diagram of the differential astigmatic method. (a) Optical path. (b) Light field distribution on FQD1 and FQD2.

to obtain:

$$\frac{r_x}{r_2} = \frac{|d - b_1|}{b_1}, \quad \frac{r_y}{r_2} = \frac{|a_1 - d|}{a_1}, \quad \frac{r_2}{r_1} = \frac{a_1}{b_0} \quad (7)$$

From Fig. 3, one can know:

$$a_1 = b_0 - l = \frac{a_0 f_1 - a_0 l + f_1 l}{a_0 - f_1} \quad (8)$$

Combining (6)–(8),  $r_x$  and  $r_y$  can be calculated as:

$$\begin{cases} r_x = r_1 \left( 1 - \frac{l(a_0 - f_1)}{a_0 f_1} \right) \left| \frac{d(a_0 - f_1)}{a_0 f_1 - a_0 l + f_1 l} + \frac{d}{f_2} - 1 \right| \\ r_y = r_1 \left( 1 - \frac{l(a_0 - f_1)}{a_0 f_1} \right) \left| 1 - \frac{d(a_0 - f_1)}{a_0 f_1 - a_0 l + f_1 l} \right| \end{cases} \quad (9)$$

Eq. (9) is the functional expression of the spot radius  $r_x$  and  $r_y$ . From the formula, it can be seen that the spot radius is affected by parameters such as  $f_1$ ,  $f_2$ ,  $d$ ,  $l$ , and  $a_0$ . In addition, since the cylindrical lens only has a focusing effect in one direction, Therefore,  $r_x$  has more term  $d/f_2$  than  $r_y$ .

## B. Principle of Differential Astigmatic Method

The above content is only the principle of astigmatic method with a detector. Since the signal directly obtained by the detector is light intensity, it is badly affected by the environment and has poor anti-noise performance. In order to improve the anti-noise performance of the astigmatic method, differential technology is added to form the differential astigmatic method. The differential astigmatic method refers to placing two detectors in front of and behind the focal plane of a cylindrical lens (shown in Fig. 4(a)). Because the spot shapes of the two detectors are not the same (shown in Fig. 4(b)), and the difference between the focus error signals of the two detectors changes with the position of the sample ( $P_s$ ). Therefore, the sample displacement change can be converted into the change of the difference between the signals of the two detectors, thereby achieving the detection of the sample defocusing displacement. The schematic diagram is as follows:

For the calculation of the differential signal value, the focus error signals of the detectors FQD1 and FQD2 can be obtained from (5) as follows:

$$FES_1 = 1 - \frac{4}{\pi} \arcsin \left( \frac{|r_{1y}|}{\sqrt{r_{1x}^2 + r_{1y}^2}} \right),$$



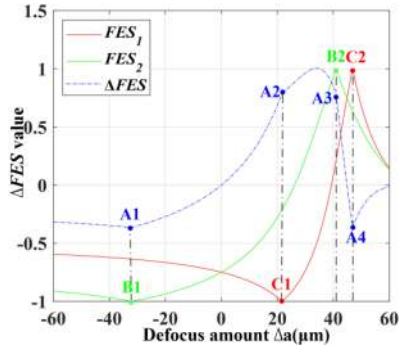


Fig. 5. FES simulation curve.

$$FES_2 = 1 - \frac{4}{\pi} \arcsin \left( \frac{|r_{2y}|}{\sqrt{r_{2x}^2 + r_{2y}^2}} \right) \quad (10)$$

Then the difference between  $FES$  values of the two detectors is:

$$\Delta FES = FES_1 - FES_2 = \frac{4}{\pi}$$

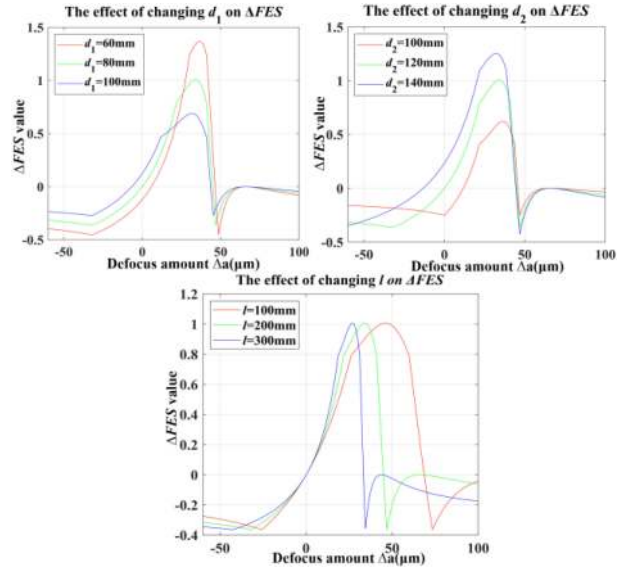
$$\left( \arcsin \left( \frac{|r_{2y}|}{\sqrt{r_{2x}^2 + r_{2y}^2}} \right) - \arcsin \left( \frac{|r_{1y}|}{\sqrt{r_{1x}^2 + r_{1y}^2}} \right) \right) \quad (11)$$

Taking the focal point ( $P_f$ , it is shown in Fig. 4(a.)) of the objective lens as the reference point (ie,  $a_0 = f_1 + \Delta a$ ), for the given system parameters  $f_1, f_2, l, d_1, d_2$  and the defocus amount  $\Delta a$  (As shown in Fig. 4(a),  $d_1$  is the distance between the FQD1 and the  $CL_0$ ;  $d_2$  is the distance between the FQD2 and the  $CL_0$ ), the relationship between the focus error signal difference ( $\Delta FES$ ) and  $\Delta a$  can be established by (9) and (11). The relationship curve is called the S curve, and its monotonous change interval can be used to detect the amount of defocus. In the differential astigmatic method, since the influence of stray light and environmental airflow disturbance on the two detectors is the same, the difference between the two can reduce the influence of the environment and improve the anti-noise ability and stability of the measurement system.

### III. SIMULATION AND ANALYSIS OF DIFFERENTIAL ASTIGMATIC METHOD

#### A. Simulation and Analysis of $\Delta FES$ Signal Curve

According to the principle of the differential astigmatic method, a measurement system of an objective lens and a cylindrical lens can solve the  $\Delta FES$  signal curve and optimize the system parameters by (9) and (11). For high-precision lithography systems, high NA objective lenses are often used for exposure, so the lens parameters are preliminarily determined as follows: objective lens focal length  $f_1 = 3.6\text{mm}$ ; objective lens radius  $r_1 = 2.9\text{mm}$ ; cylindrical lens focal length  $f_1 = 100\text{mm}$ . According to (9) and (11), the simulated S curve shown in Fig. 5 can be obtained. The red curve in the figure represents the focus error signal curve ( $FES_1$ ) of the detector FQD1 position, and the green curve represents the focus error signal curve ( $FES_2$ ) of the detector FQD2 position. The difference between the two is represented by the blue dashed line, which represents the

Fig. 6. The influence of system parameters  $d_1, d_2$ , and  $l$  on the  $\Delta FES$  curve.

differential signal curve ( $\Delta FES$ ). It can be seen from the graph that there are maximum points (ie, B2 and C2) and minimum points (ie, B1 and C1) for the  $FES$  curve of a single detector, which correspond to the horizontal focal line and the vertical focal line respectively. This is in line with the analysis of (5) above. The  $\Delta FES$  curve is divided into 5 sections by these 4 extreme points, and the A1A2 section and A3A4 section both have a monotonic interval with good linearity, and both can be used as the effective interval for sample displacement measurement.

It can be seen from (9) and (11) that the system parameters  $l, d_1$  and  $d_2$  all have an effect on the  $\Delta FES$  curve, so simulation verifications were performed on them respectively, as shown in Fig. 6. It can be seen that the smaller  $d_1$  and the larger  $d_2$ , the steeper the  $\Delta FES$  curve and the larger the range of its linear interval; the smaller  $l$ , the steeper the  $\Delta FES$  curve, but the range of its linear interval will be limited. Therefore, taking the experimental requirements as the constraint condition and combining (9) and (11), the system parameters with maximum sensitivity can be solved to obtain the optimal focal plane measurement.

#### B. Solve Optimal System Parameters

In the field of high-precision lithography, since the focal depth of the high NA objective lens is about  $1\ \mu\text{m}$ , the focusing system is usually required to have a defocus detection range of at least  $5\ \mu\text{m}$ . Therefore, the value range of the linear interval  $L$  is initially set as:  $L \geq 5\ \mu\text{m}$ . Considering the influence of the size of the light spot on the detector on the detection accuracy, too small a light spot may cause the detector to be insensitive and unable to effectively detect signal changes. At the same time, it also requires the system to have high assembly accuracy. If the light spot is too large, it may exceed the detection range of the detector, and the detector can only receive part of the light, which seriously affects the signal detection. Therefore, it

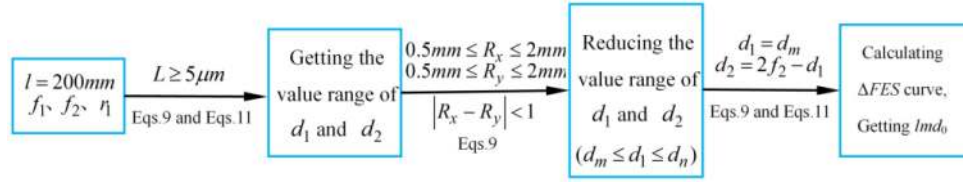


Fig. 7 Flow chart of system parameter optimization algorithm.

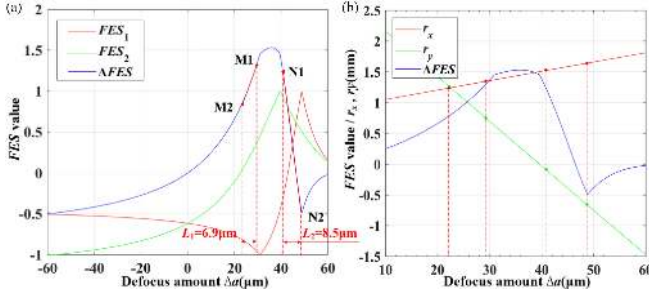


Fig. 8. Solution results. (a) The simulated  $\Delta FES$  curve and its linear interval. (b) The curves of  $r_x$  and  $r_y$  varying with the defocus amount.

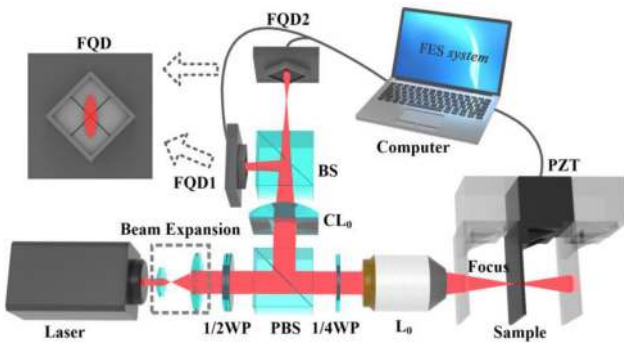


Fig. 9. Experimental schematic diagram of the defocus detection system based on differential astigmatic method.

is necessary to reasonably set the maximum radius  $R_x$  and  $R_y$  of the elliptical spot in the  $x$  and  $y$  directions. Since the pupil radius of the high NA objective lens in the experiment is 2.9mm, and the target surface size of the four-quadrant detector is 5mm $\times$ 5mm, it can be defined as follows:  $0.5\text{mm} \leq R_x \leq 2\text{mm}$ ;  $0.5\text{mm} \leq R_y \leq 2\text{mm}$ ; To reduce the interference of external stray light, the requirements are as follows:  $R_x \approx R_y$  (ie,  $|R_x - R_y| < 1$ ). In order to reduce costs and save space, the entire measurement system is required to have a compact structure, so the system parameters are set as follows:  $l \leq 200\text{mm}$ ,  $d_1 \leq 150\text{mm}$  and  $d_2 \leq 150\text{mm}$ .

According to the above conditions, the algorithm shown in Fig. 7 is designed to optimize the system parameters. It can be seen from Fig. 6 that the change of  $l$  has little effect on the A1A2 section of the  $\Delta FES$  curve. In the A3A4 section, the greater the  $l$ , the higher the sensitivity, that is, for a measurement system that meets the experimental requirements, the  $l$  should be as large as possible. Therefore, the initial value is taken as:  $l = 200\text{mm}$ . And using the system initial values  $f_1, f_2, r_1$ , combined with Eq. and (11), in the A1A2 and A3A4 sections of the curve in Fig. 5, with the detection range  $L$  as the limiting condition, the value

range of  $d_1$  and  $d_2$  can be preliminarily determined (in order to reduce parameter variables, the positions of the two detectors are symmetrical about the focal plane of the cylindrical lens, ie,  $d_1 + d_2 = 2f_2$ ). Secondly, the radius of the detector is used as a limiting condition to further narrow the range of values of  $d_1$  and  $d_2$ . Finally, find the system parameters value with the highest sensitivity (Its value is represented by the variable  $lmd_0$ ) in this range. It can be seen from Fig. 6 that the smaller  $d_1$  and the larger  $d_2$  value, the greater the linear range and sensitivity of  $\Delta FES$ , so finally take the  $d_1$  and  $d_2$  calculated in the previous step as the final parameter values of the system. As for the quantification standard of sensitivity, considering that astigmatism focusing systems generally measure small displacements, the midpoint position derivative of the linear monotonic interval of the  $\Delta FES$  curve is used to characterize the sensitivity.

Solved by algorithm, the results are as follows:  $l = 200\text{mm}$ ,  $d_1 = 70\text{mm}$ ,  $d_2 = 130\text{mm}$ . The simulation result is shown in Fig. 8, and the  $\Delta FES$  curve is the blue curve in the figure. The slope on both sides of the curve peak is steep, indicating that the system has high sensitivity; the interval with good linearity on both sides is taken as the effective interval for sample defocus measurement, as shown in the M1M2 section ( $L_1 = 6.9\mu\text{m}$ ) and N1N2 section ( $L_2 = 8.5\mu\text{m}$ ) in Fig. 8(a). It can meet the needs of the defocus detection range of the high NA lithography system. The changes in the radius of the spot in the  $x$  and  $y$  directions with the defocus amount are shown in Fig. 8(b). The maximum radius  $R_x$  and  $R_y$  in the linear range are both greater than 0.5mm and less than 2mm, which meets the requirements of the four-quadrant detector target surface.

#### IV. EXPERIMENTAL SYSTEM AND RESULT DISCUSSION

In order to verify the simulation optimization results, a defocus detection system based on differential astigmatic method as shown in Fig. 9 was built for experiments. In our experiment, the laser source (Laser) emits a light beam with a wavelength of 633nm. After the beam is collimated and expanded by the beam expander, the polarization direction is adjusted by the 1/2 wave plate (1/2WP). After passing through the polarization beam splitter (PBS), 1/4 wave plate (1/4WP) and objective lens ( $L_0$ ), the light beam is focused on the sample. The light reflected from the sample surface passes through  $L_0$ , 1/4WP, cylindrical lens ( $CL_0$ ) and the beam splitter prism (BS), and received by the four-quadrant detectors FQD1 and FQD2 respectively. At the same time, the sample is mounted on the PZT (Nanometer precision micro-motion stage), which can move axially at nanometer level, and can form feedback through the focus error

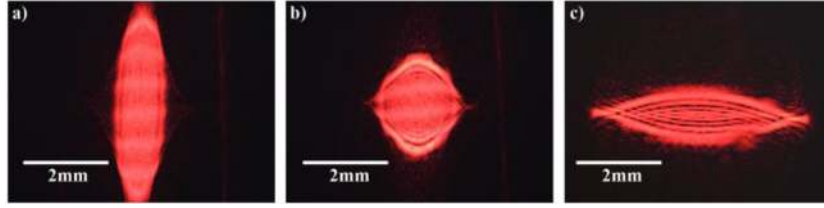


Fig. 10. The changes in the shape of the light spot during the axial displacement of the sample.

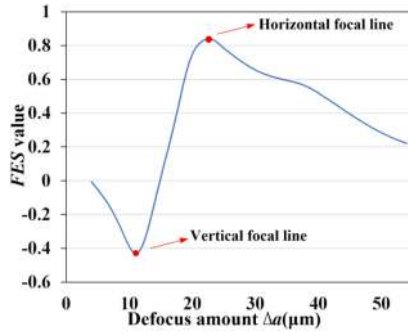


Fig. 11. FES curve collected by an FQD.

signal  $FES$  obtained by the four-quadrant detector. According to theoretical calculations and application requirements in the field of high-precision lithography machines, the parameters are selected as follows:  $L_0$  selects a Nikon objective lens ( $NA = 0.8$ ), and its focal length is approximately as follows:  $f_1 = 3.6\text{mm}$ ; the focal length of  $CL_0$  is as follows:  $f_2 = 100\text{mm}$ ; the distance between  $L_0$  and  $CL_0$  is taken as follows:  $l = 200\text{mm}$ ; the distances between  $CL_0$  and the detectors are as follows:  $d_1 = 70\text{mm}$ ,  $d_2 = 130\text{mm}$ .

#### A. FES Curve Test and Verification

First, the experiment about the astigmatic method of a detector was carried out. Fig. 10 shows the changes of the spot shape on an FQD. When the sample is axially displaced, the shape of the spot changes to a vertical ellipse (shown in Fig. 10(a)), a circle (shown in Fig. 10(b)), and a horizontal ellipse (shown in Fig. 10(c)) in turn. The  $FES$  curve is shown in Fig. 11. It can be seen that there are two extreme points corresponding to the meridian focal line and the horizontal focal line. The experimental phenomena and key points are basically consistent with the simulation calculation results. There is a certain gap between the experimental results and the simulation, because there are aberrations in the experimental system and the experimental beam is the Gaussian beam, the spot shape corresponding to the extreme point is not a strict focal line on the detector but an elliptical spot (ie, the absolute value of the  $FES$  value corresponding to the extreme point is less than 1).

Then, based on the differential principle, two FQDs (FQD1 and FQD2) were used to collect signals, and the experiment of differential astigmatic method was performed, and the differential signal  $\Delta FES$  curve was obtained, as shown in Fig. (12). Fig. 12(a) and (b) show the curve of the signal intensity of each quadrant of FQD1 and FQD2 changing with the defocus

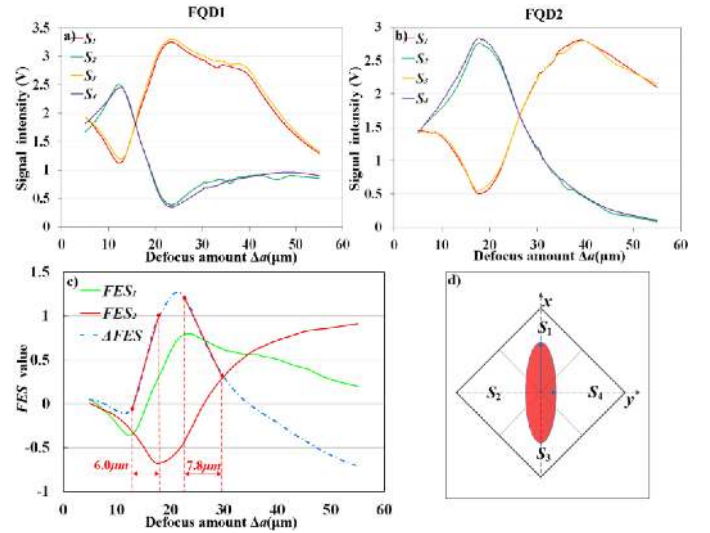


Fig. 12. Experimental results of the differential astigmatic method. (a) The signal changes of each quadrant in FQD1 (b) The signal changes of each quadrant in FQD2 (c) The curves of  $FES_1$ ,  $FES_2$ , and  $\Delta FES$  varying with  $\Delta a$  (d) The division of FQD photosensitive target surface.

amount ( $\Delta a$ ) of the sample. One can see that the signal intensity curve collected by quadrant  $S_1$  of each FQD and the curve of quadrant  $S_3$  almost overlap, and the signal intensity curve collected by quadrant  $S_2$  and the curve of quadrant  $S_4$  almost overlap, indicating that the light spot is located in the center of the FQD and its shape change is symmetrical and uniform. Fig. 12(c) shows the curves of  $FES_1$ ,  $FES_2$  and  $\Delta FES$  changing with the defocus amount. One can see that the curve is consistent with the characteristics of the simulation curve shown in Fig. 8, and is divided into 5 sections, and there are sections on both sides of the wave crest with good linearity; the maximum linear range is  $6.0\mu\text{m}$  and  $7.8\mu\text{m}$  respectively; the result is basically consistent with the theoretical calculation. The slight difference between the experimental  $\Delta FES$  curve and the simulation curve is due to the influence of aberration and the gap between the FQD quadrants, which limits the change of  $FES_1$  and  $FES_2$ , thereby affecting the change of  $\Delta FES$  curve. It should be noted that the simulation curve was obtained by using the objective lens focal point as the reference point for positive defocusing and negative defocusing displacement, while the position of the focal plane was uncertain during the experiment, and the defocusing displacement can only be carried out in one direction, so the abscissa value of the experimental curve was positive.



TABLE I  
DYNAMIC REPEATABILITY MEASUREMENT POINT POSITION VALUE WITHIN 1 HOUR ( $\mu\text{m}$ )

$\Delta FES \setminus T(\text{min})$	0	8	16	24	32	40	48	56	64
$\Delta FES_1 = -0.0773$	-8.965	-8.975	-8.975	-8.975	-8.980	-8.991	-8.988	-8.995	-8.999
$\Delta FES_2 = -0.0290$	-8.501	-8.496	-8.510	-8.503	-8.512	-8.517	-8.523	-8.525	-8.531
$\Delta FES_3 = 0.0410$	-8.035	-8.040	-8.042	-8.044	-8.046	-8.061	-8.061	-8.065	-8.720

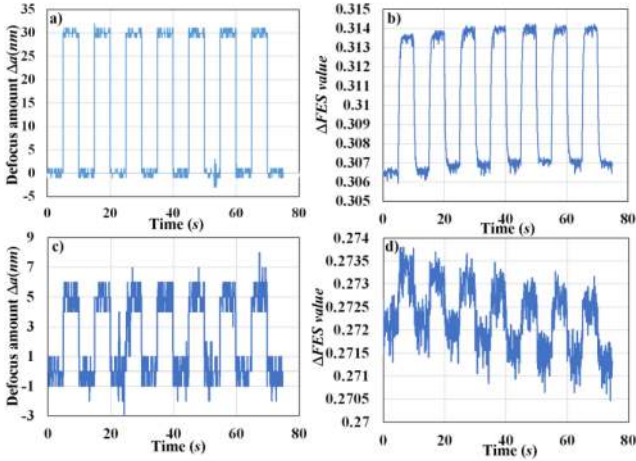


Fig. 13. Accuracy detection of the square wave signal. (a) A square wave signal (signal 1) with an amplitude of 30nm. (b) The FES curve of the signal 1. (c) A square wave signal (signal 2) with an amplitude of 5nm. (d) The FES curve of the signal 2.

### B. The Sensitivity Test of the Differential Astigmatic Detection System

To test the sensitivity of our experimental system, another experiment was carried out. In the experiment, a square wave signal was input to the PZT, and the sample was moved along the optical axis at a certain frequency, which caused the sample to defocus. This causes  $FES$  to change with time, as shown in Fig. 13. Input the square wave signal shown in Fig. 13(a) to the PZT controller to make the sample vibrate axially with an amplitude of 30nm, that is, the defocus amount changes with an amplitude of 30nm. Use the detection system established in Fig. 9 to conduct experiments. Fig. 13(b) shows the experimental results. One can see that the  $FES$  value also undergoes significant periodic changes over time, and the output waveform is basically the same as the input waveform, indicating that the defocus detection system can accurately detect the focus distance of 30nm. Fig. 13(c) reduces the input signal amplitude to 5nm. The measurement result is shown in Fig. 13(d). One can see that the  $FES$  value changes periodically with time, indicating that the system can also detect the defocus amount of 5nm. The drift of the experimental curve was due to the influence of air disturbance and environmental vibration.

### C. Repeatability Tests of the Defocus Detection System

For the field of high-precision focal plane detection, not only the defocusing detection system is required to have good sensitivity, but also to have high repeat positioning accuracy. As shown in Fig. 13(d), one can see that the measurement system has drift. Therefore, three points were taken on the curve in Fig. 12 and the dynamic repeatability displacement experiment

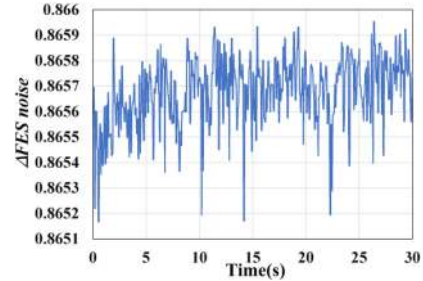


Fig. 14. The curve of  $\Delta FES$  changing with time (the PZT keeps static and motionless).

was carried out. Control the precision micro-motion stage PZT to move the sample, make the detector measurement signal  $\Delta FES$  equal to  $-0.0773$ ,  $-0.029$ ,  $0.0410$ , and record the corresponding PZT position value, the interval is 8 minutes, a total of 9 groups are taken, as shown in Table I. It can be seen that the drift amount within one hour is 30nm, indicating that its repeat positioning accuracy is high, and its repeat positioning accuracy reaches 30 nm within one hour.

In addition to dynamic repeatability, repeat positioning accuracy also includes static repeatability, that is, when the PZT does not move, it measures the drift of  $\Delta FES$  value of the defocus detection system (ie, the noise of system). As shown in Fig. 14, one can see that  $\Delta FES$  changes randomly within the range of 0.001, which is converted into the change of the defocus amount in the range of 10nm, indicating that the defocus detection system has good static repeatability. At the same time, one can see that the above experimental results are all produced by PZT, not from noise, and the results are accurate. Therefore, our defocus detection system has a comprehensive repeat positioning accuracy of up to 30nm and can respond accurately to the defocus amount of 30nm, which can meet the defocus detection requirements in the field of high-precision lithography machines.

### D. Noise Tests of the Defocus Detection System

Finally, in order to test the noise resistance and stability of the system of differential astigmatic method, we conducted a comparison experiment between the differential astigmatic system and the single-channel astigmatic system. The PZT keeps static and motionless. We use a laser with adjustable power, change its power during the experiment, and measure the static repeatability of the two detection systems. The results are shown in Fig. 15. Fig. 15(a) and (b) are the static repeatability curves of the single-channel astigmatic system, the  $FES$  value of which has a variation range of 0.016, indicating that it has the obvious noise. Fig. 15(c) is the static repeatability curves of the differential

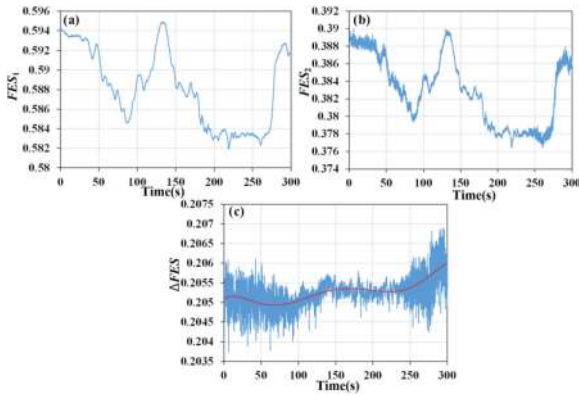


Fig. 15. Comparison of noise curves of the single-channel astigmatic system and the differential astigmatic system. (a) Noise curve of the single-channel astigmatic system 1 (received by detector FQD1). (b) Noise curve of the differential astigmatic system 2 (received by detector FQD2). (c) Noise curve of the differential astigmatic system.

astigmatic system. And the variation range of differential signal  $\Delta FES$  value is only 0.003, which is far less than the noise of the single-channel astigmatic system. It is verified that the differential astigmatic system has better noise resistance and better stability.

## V. CONCLUSION

In this work, the high NA defocus detection system is analyzed, simulated and verified by experiments using the theory of astigmatism combined with the principle of differential technology. On the premise of taking into account the practical feasibility, through theoretical analysis and algorithm simulation, the system parameters with maximum sensitivity was solved. And for the objective lens with a numerical aperture of 0.8, an experimental system was established for experimental verification and repeated positioning accuracy measurement. The experimental results show that the high NA defocus detection system has a good linear relationship. Its linear range can reach  $6.0\mu\text{m}$  and  $7.8\mu\text{m}$ . The system sensitivity is 5 nm, and its repeatability accuracy can reach 30 nm. It has better noise resistance and stability than the single-channel astigmatic defocus detection system. Theoretical and experimental results show that under the premise of considering feasibility and experimental requirements, the research of this high NA defocus detection system can be applied to the field of new high-precision lithography machines to meet its high-precision defocus detection requirements.

## ACKNOWLEDGMENT

The authors thank L.L for assistance during the experiment.

## REFERENCES

- [1] Q. Li *et al.*, "Sapphire-based fresnel zone plate fabricated by femtosecond laser direct writing and wet etching," *IEEE Photon. Technol. Lett.*, vol. 28, no. 12, pp. 1290–1293, Jun. 2016.
- [2] Y.-H. Yu, Z.-N. Tian, T. Jiang, L.-G. Niu, and B.-R. Gao, "Fabrication of large-scale multilevel phase-type fresnel zone plate arrays by femtosecond laser direct writing," *Opt. Commun.*, vol. 362, pp. 69–72, 2016.
- [3] L. Liu *et al.*, "Generation of an ultra-long optical needle induced by an azimuthally polarized beam," *IEEE Photon. J.*, vol. 13, no. 1, Feb. 2021, Art. no. 1500912.

- [4] T. Wei, J. Wei, K. Zhang, and L. Zhang, "Image lithography in telluride suboxide thin film through controlling "virtual" bandgap," *Photon. Res.*, vol. 5, no. 1, pp. 22–26, 2017.
- [5] N. Park, Y. Park, K. Park, and H. Yang, "Applications of next generation optical data storage technologies," *IEEE Trans. Magn.*, vol. 47, no. 3, pp. 669–678, Mar. 2011.
- [6] D. Huerta-Murillo *et al.*, "Fabrication of multi-scale periodic surface structures on Ti-6Al-4V by direct laser writing and direct laser interference patterning for modified wettability applications," *Opt. Lasers Eng.*, vol. 98, pp. 134–142, 2017.
- [7] Y. Zhang, Z. Zhang, C. Geng, S. Xu, T. Wei, and W. Bi, "Versatile nanosphere lithography technique combining multiple-exposure nanosphere lens lithography and nanosphere template lithography," *Chin. Opt. Lett.*, vol. 15, no. 6, 2017, Art. no. 062201.
- [8] H. G. Rhee, D. Kim, S. K. Hong, and Y. W. Lee, "300 mm reference wafer fabrication by using direct laser lithography," *Rev. Sci. Instrum.*, vol. 79, no. 10, Oct. 2008, Art. no. 103103.
- [9] C. H. Liu and Z. H. Li, "Application of the astigmatic method to the thickness measurement of glass substrates," *Appl. Opt.*, vol. 47, no. 21, pp. 3968–3972, Jul. 2008.
- [10] Z. Guangya, S. Yibing, H. Xiyun, and Y. Guoguang, "Studies on high precise astigmatic focus error detect system," *J. Zhejiang Univ.*, vol. 32, no. 6, pp. 46–50, Nov. 1998.
- [11] H. G. Rhee, D. I. Kim, and Y. W. Lee, "Realization and performance evaluation of high speed autofocusing for direct laser lithography," *Rev. Sci. Instrum.*, vol. 80, no. 7, Jul. 2009, Art. no. 073103.
- [12] L. Li, C. Kuang, D. Luo, and X. Liu, "Axial nanodisplacement measurement based on astigmatism effect of crossed cylindrical lenses," *Appl. Opt.*, vol. 51, no. 13, pp. 2379–2387, May 2012.
- [13] X. Liang, Z. Bai, and J. Wei, "Movement flatness error measurement based on an astigmatic method," *Appl. Opt.*, vol. 56, no. 15, pp. 4347–4352, 2017.
- [14] Z. Bai and J. Wei, "Focusing error detection based on astigmatic method with a double cylindrical lens group," *Opt. Laser Technol.*, vol. 106, pp. 145–151, 2018.
- [15] Y. Li, K. Wu, and Z. Ai, "A circuit design of high-precision micro-displacement sensor system for DVD pickup head," in *Proc. Symp. Photon. Optoelectron.*, May 2012, pp. 1–4.
- [16] D. E. Denk and A. G. Polshchuk, "Methods of improving the accuracy of operation of an autofocus in a circular laser writing system," *Optoelectron. Instrum. Data Process.*, vol. 46, no. 1, pp. 87–95, 2010.
- [17] Y. Tian, T. Jiang, P. Gao, M. Jiang, H. Guo, and S. Zhuang, "Design for parameters of astigmatic lens in defocus detection based on astigmatic method," *Guangxue Jishu/Opt. Technique*, vol. 38, pp. 435–440, 2012.
- [18] C. Li, W. Junhua, and X. Min, "Analysis and calibration of defocus detection system based on astigmatism method," *Laser Optoelectron. Prog.*, vol. 53, 2016, Art. no. 051205.
- [19] I. A. Martínez and D. Petrov, "Back-focal-plane position detection with extended linear range for photonic force microscopy," *Appl. Opt.*, vol. 51, no. 25, pp. 5973–5977, Sep. 2012.
- [20] C. Di, W. Yan, S. Hu, F. Xu, and J. Li, "Technology of focus detection for 193 nm projection lithographic tool," in *Proc. SPIE Int. Soc. Opt. Eng.*, 2012, p. 84180Y.
- [21] S. Zhou, S. Wang, J. Chen, G. Rui, and Q. Zhan, "Creation of radially polarized optical fields with multiple controllable parameters using a vectorial optical field generator," *Photon. Res.*, vol. 4, no. 5, pp. B35–B39, 2016.
- [22] Y. Zhou *et al.*, "Self-starting passively mode-locked all fiber laser based on carbon nanotubes with radially polarized emission," *Photon. Res.*, vol. 4, no. 6, pp. 327–330, 2016.
- [23] T. Liu, J. Tan, and J. Liu, "Tighter focusing of amplitude modulated radially polarized vector beams in ultra-high numerical aperture lens systems," *Opt. Commun.*, vol. 294, pp. 21–23, 2013.
- [24] J. Ma, H. Sun, S. Wang, and D. Yan, "Effects of atmospheric turbulence on photodetector arrays," *Appl. Opt.*, vol. 28, no. 11, pp. 2123–2126, Jun. 1989.
- [25] M. Toyoda, K. Araki, and Y. Suzuki, "Wave-front tilt sensor with two quadrant detectors and its application to a laser beam pointing system," *Appl. Opt.*, vol. 41, no. 12, pp. 2219–2223, 2002.
- [26] W. Zhao, C. Liu, and L. Qiu, "Laser divided-aperture differential confocal sensing technology with improved axial resolution," *Opt. Exp.*, vol. 20, no. 23, pp. 25979–25989, Nov. 2012.
- [27] Y. Wang, L. Qiu, and W. Zhao, "High precision radially-polarized-light pupil-filtering differential confocal measurement," *Opt. Laser Technol.*, vol. 82, pp. 87–93, 2016.
- [28] Q. Hao, J. Cao, Y. Hu, Y. Yang, K. Li, and T. Li, "Differential optical-path approach to improve signal-to-noise ratio of pulsed-laser range finding," *Opt. Exp.*, vol. 22, no. 1, pp. 563–575, Jan. 2014.